

NUMERICAL SIMULATION OF CRYSTALLIZATION FOULING TAKING INTO ACCOUNT FOULING LAYER STRUCTURES

J. Xiao*, J. Han, F. Zhang, and X.D. Chen*

Suzhou Key Laboratory of Green Chemical Engineering
School of Chemical and Environmental Engineering
College of Chemistry, Chemical Engineering and Materials Science
Soochow University, Suzhou, Jiangsu Province 215123, China

*Corresponding authors: jie.xiao@suda.edu.cn (J. Xiao) and xdchen@suda.edu.cn (X.D. Chen)

ABSTRACT

The fouling layers on heat exchanger surfaces exhibit complicated structures, which essentially determine flow hydrodynamics, fouling kinetics and hence the heat transfer performance. Numerical models developed so far for the fouling process, however, are based exclusively on the assumption of an impermeable fouling layer with a uniform porous structure. In order to quantitatively evaluate the effect of fouling layer structure on fouling dynamics, this work systematically investigated four representative schemes for fouling layer characterization: i.e., a homogeneous porous medium that is impermeable to water (HoIm), a heterogeneous porous medium that is impermeable to water (HeIm), a homogeneous porous medium that is permeable to water (HoPe), and a heterogeneous porous medium that is permeable to water (HePe). Under the same operational conditions, four models offer significantly different prediction results on the fluid velocity, temperature distribution and fouling resistance. It is concluded that numerical model development should take the fouling layer structure into account, and the scheme of HePe that best resembles a real fouling layer structure should be a promising option.

Keywords: crystallization fouling; fouling layer structure; numerical modeling; heterogeneous porous media

INTRODUCTION

The morphology and structure of fouling layers formed on a heat exchanger surface influence deposit properties, the heat, mass and momentum transfer in the fluid phase, as well as the heat and mass exchange between the deposit and the fluid (Zhao and Chen, 2013). In-depth understanding of deposit layer formation and its structural effects on the fouling process could lead to effective fouling mitigation or even prevention strategies. These exploration tasks, however, are not trivial due to a lack of knowledge of the crystallization process and the complicated deposit structure. Our understanding of crystal nucleation, especially heterogeneous nucleation on a surface, is far from complete (Anwar and Zahn, 2011; Xiao and Chaudhuri, 2012). The growth of crystal is even more complicated since mineral crystals usually possess different anhydrous polymorphs (Zhao and Chen, 2013). Calcium carbonate (CaCO_3), for instance, has three major polymorphs, namely, calcite, aragonite and vaterite. A slight modification of well controlled experimental conditions including temperature, flow velocity and pH may

result in a completely different crystal structure (Andritsos et al., 1997). A variety of crystal shapes can be simultaneously identified in a CaCO_3 layer including prismatic needles/rods, flower, sand-rose, half-moon, and rhombic/hexagonal (Quddus and Al-Hadhrani, 2009). The stock solution may contain multiple minerals, which leads to composite and particulate fouling, and hence a more complicated deposit structure (Zhang et al., 2013; Zhao and Chen, 2013). Furthermore, deposit structures and properties evolve throughout the complete fouling process (Andritsos et al., 1997; Kim et al., 2002). Although advanced experimental techniques such as X-ray diffraction (XRD) and scanning electron microscopy (SEM) have been widely used to characterize and visualize the final deposit structure (Andritsos et al., 1997; Zhou and Zhang, 2010; Paakkonen et al., 2012), it is a challenging task to track crystal nucleation and growth dynamics. Quantitative evaluation of the consequences of structural evolution becomes even more challenging from an experimental point of view.

In addition to experimental efforts, mathematical models have been developed and continuously improved to help us understand each stage of the complex fouling process, i.e., initiation, transport, attachment, removal and ageing (Bohnet, 1987). Yang et al. (2012) developed a very simple lumped parameter model to correlate fouling resistance with the surface coverage of crystals in the initiation/induction stage. A more comprehensive model for the induction period was developed by Mayer et al. (2013). The model is capable of predicting the induction time by assuming cubic shaped crystals in the system. Ishiyama et al. (2010 and 2011) and Coletti et al. (2010) investigated the ageing stage and explored the effect of ageing on thermal and hydraulic performance of heat transfer devices. Ageing was expressed in the model via a change in the deposit property, i.e., thermal conductivity. The other three stages have been vigorously investigated as well. Bohnet and his group (Brahim et al., 2003, 2004; Bohnet, 2005) have been developing numerical models for the crystallization fouling. Momentum, mass and heat conservations equations in the fluid phase over a fouling layer were coupled. A scheme called "fictitious crystal growth" was proposed to implicitly deal with the geometrical evolution of the flow model, where crystal growth led to the increase of the flow velocity only and the velocity was calculated based on continuity conditions (Brahim et al., 2003). Very recently, Zhang et al. (2015) reported a pseudo-dynamic approach to explicitly tackle geometrical evolution of the fouling layer. This

unique method allows us to track dynamic evolution of the deposit surface and its intricate interactions with hydrodynamics and fouling kinetics.

Although the models reported so far can take fouling layer growth into account either implicitly or explicitly, they over-simplified the fouling layer structure. Two assumptions were conventionally adopted: the fouling layer is a homogeneous porous medium and the layer is impermeable to the fluid flow (Brahim et al., 2003, 2004; Bohnet, 2005; Zhang et al., 2015). It remains unclear whether the model with these simplifications could sufficiently characterize a realistic fouling process. The main objective of this work is to quantitatively evaluate the effects of simplified deposit structures on the fouling process. At the same time, a simple but effective structural approximation scheme should be identified that would better resemble the fouling layer structure (in the growth stage) and hopefully can be integrated into a numerical model for crystallization fouling in the future. It should be pointed out that deposit structures also play an important role in the initiation and ageing stages, which is beyond the scope of this paper.

MODELING METHODOLOGY

As stated in the introduction part, the fouling layer was conventionally modelled as a homogeneous porous layer. Although the effective properties of this layer were calculated with consideration of properties of the liquid in the pores, the fluid cannot flow through this layer (see the deposit domain Ω_f in Fig. 1(a)). This characterization scheme is denoted as HoIm in this work. Realistic fouling layers imaged by the SEM technique demonstrate much more complicated structures (Andritsos et al., 1997; Brahim et al., 2003). In most cases, a layered structure can be identified and the fluid should be able to flow through the spaces between crystals in the deposit domain (see the SEM image in Fig. 1(e) taken from Brahim et al. (2003)). In order to mimic the realistic structure, the other three schemes have been introduced to gradually relax the conventionally adopted assumptions. Figure 1 (b) gives a scheme denoted as HeIm, where the fouling layer is a heterogeneous porous medium that is impermeable to the fluid flow. Figure 1 (c) and (d) show schemes that allow fluid flow through the fouling layer. One assumes a homogeneous porous structure (i.e., HoPe in Fig. 1(c)) and the other takes the heterogeneous structure into account (i.e., HePe in Fig. 1(d)). Moreover, the heterogeneous structures in HeIm and HePe schemes are assumed to be a four-layer structure with each layer having the same volume but different porosities. As suggested by the SEM image, a layer closer to the heat exchanger surface has a lower porosity value. These four representative structures will be investigated in this work to demonstrate the impact of fouling layer structures on heat and momentum transfer in the system. The influence on mass transfer and fouling kinetics, however, will be qualitatively discussed only. In order to offer a fair comparison, the volume average porosity in HeIm and HePe schemes is set equal to the porosity in HoIm and HoPe schemes.

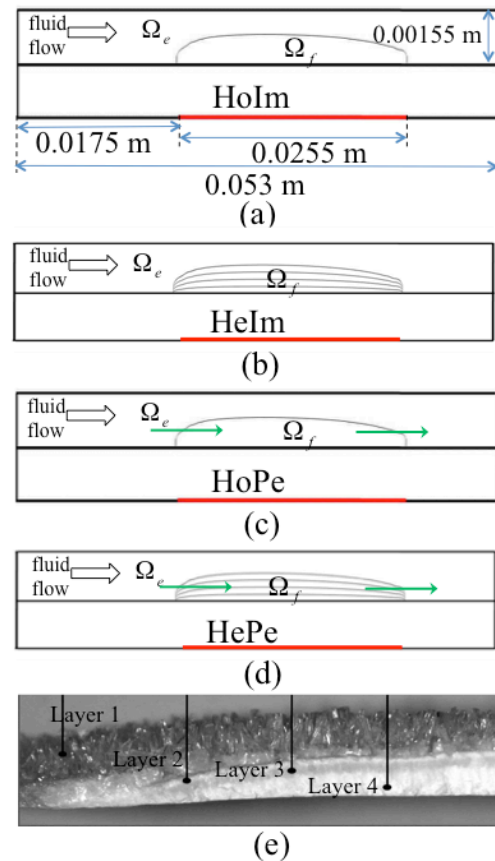


Fig. 1. Approximation schemes for fouling layer characterization: (a) a homogeneous porous layer, impermeable to the fluid flow, denoted as HoIm, (b) a heterogeneous porous layer, impermeable to the fluid flow, denoted as HeIm, (c) a homogeneous porous layer, permeable to the fluid flow, denoted as HoPe, (d) a heterogeneous porous layer, permeable to the fluid flow, denoted as HePe, and (e) an SEM image of a fouling layer structure (taken from Brahim et al. 2003).

As a first step, the *in silico* experiments will be performed in the laminar flow regime. Note that the investigation of the laminar flow regime is of practical significance, especially for fouling in microstructured devices (Schoenitz *et al.*, 2015). Detailed model descriptions for the system with the HoIm scheme can be found in Zhang et al. (2015), which are omitted here. The same model can be used to simulate the HeIm system, where the only difference is that the porosity of the deposit layer is now location dependent. Simulation models for the other two systems, i.e., HoPe and HePe, are significantly different due to the incorporation of a permeable fouling layer. New models have to be established to describe a porous media flow together with conductive and convective heat transfer in the fouling layer. Again, this work focuses on the structural effect on momentum and heat transfer only.

Governing Equations for Momentum Transfer

Momentum transfer models for the systems given in Fig. 1(c) and (d) should be able to describe free media flow in the solution domain Ω_e coupled with porous media flow

in the fouling layer domain Ω_f . One frequently used approach is to couple the Navier-Stokes equation with Darcy's law. However, this simple method cannot characterize the fluid flow behavior in the region close to the free-porous media flow interface, since the viscous effects arising from the free media flow cannot be taken into account sufficiently well. As an extension of Darcy's law, the Brinkman equations can take care of the macroscopic viscous effect in free media flow as well as the microscopic shear effects inside pore channels (Durlafsky and Brady, 1987). Thus, in this work, the systems with coupled free and porous media flow have been modeled using the Navier-Stokes equation together with the Brinkman equation.

The continuity equation for an incompressible flow in the complete simulation domain is:

$$\nabla \cdot \vec{u} = 0 \quad (1)$$

Flow in the solution domain Ω_e is described by the standard Navier-Stokes equation:

$$\rho_w (\vec{u} \cdot \nabla) \vec{u} = \nabla \cdot [-p\vec{I} + \mu(\nabla\vec{u} + (\nabla\vec{u})^T)] \quad (2)$$

where ρ_w is the density of the fluid (kg/m^3); \vec{u} is the fluid velocity (m/s); p is the pressure (Pa); μ denotes the dynamic viscosity of the fluid (Pa·s). The left-hand side of the equation represents convective momentum transfer in free media flow.

Porous media flow in domain Ω_f is modeled using the Brinkman equation with a Forchheimer correction:

$$\frac{\mu}{k} \vec{u} = \nabla \cdot [-p\vec{I} + \frac{\mu}{\omega} (\nabla\vec{u} + (\nabla\vec{u})^T)] - \frac{\rho_w \omega C_f}{\sqrt{k}} \vec{u} |\vec{u}| \quad (3)$$

where ω is the porosity of the deposit layer that can be location dependent. k denotes the permeability of the porous medium (m^2), which is related to the porosity by the following equation (Borisova and Adler, 2005):

$$k = k_0 \left(\frac{\omega}{\omega_0} \right)^{3.55} \quad (4)$$

where k_0 and ω_0 are respectively the permeability and the porosity of the porous media at a reference state. The dimensionless friction coefficient C_f is (Amiri and Vafai, 1998):

$$C_f = \frac{1.75}{\sqrt{150\omega^3}} \quad (5)$$

The last term on the right-hand side of Eq. (3) represents the Forchheimer correction for turbulent drag contributions.

Governing Equations for Heat Transfer

Heat transfer in the solution domain Ω_e and the fouling layer domain Ω_f can be modelled using a general governing equation:

$$(\rho C_p)_{eq} \vec{u} \cdot \nabla T = \nabla \cdot (\lambda_{eq} \nabla T) \quad (6)$$

where T is the temperature (K); the equivalent volumetric heat capacity of the solid-fluid system is calculated through:

$$(\rho C_p)_{eq} = \rho_s C_{p,s} (1 - \omega) + \omega \rho_w C_{p,w} \quad (7)$$

where ρ_s is the density of the deposit solid (kg/m^3); $C_{p,s}$ and $C_{p,w}$ are respectively the specific heat capacity of the solid and the fluid (J/(kg·K)). Similarly, the equivalent thermal conductivity of the solid-fluid system is related to the solid conductivity λ_s and the fluid conductivity λ_w by:

$$\lambda_{eq} = \lambda_s (1 - \omega) + \omega \lambda_w \quad (8)$$

When the porosity ω is set to 1, Eq. (6) should be able to describe convective heat transfer in free media flow as well. Also note that the velocity in Eq. (6) should be derived by solving Eqs. (1) and (2). In this way, momentum transfer can be coupled with heat transfer.

Boundary Conditions

Momentum conservation equations should be solved for the solution domain Ω_e and the fouling layer domain Ω_f . As shown in Fig. 2, the fluid enters the flow channel at a constant velocity v_{in} and leaves the channel from the exit where the gauge pressure is 0. Non-slip boundary condition is specified for the substrate surface and the top wall of the flow channel. In order to couple free media flow in Ω_e and porous media flow in Ω_f , flow continuity is specified on the free-porous media flow interface.

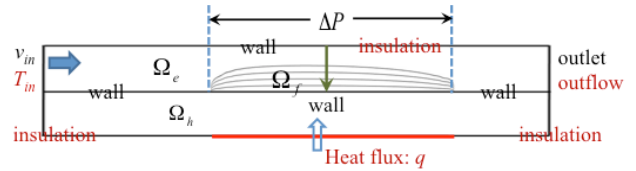


Fig. 2. The fouling simulation system with boundary conditions for heat and momentum conservations.

Heat transfer takes place in the complete simulation system including the domain of substrate metal Ω_h (see Fig. 2). The fluid inlet temperature is kept at T_{in} . The outflow of heat at the exit is convection dominant. A constant influx q is set for a part of the heat transfer surface shown in red in Fig. 2. All other boundaries are insulated walls.

Fouling Resistance Quantification

Different schemes for fouling layer characterization could lead to different heat transfer behaviours, and hence different fouling resistance values. The fouling resistance can be calculated as the ratio of the difference between the temperatures of a fouled surface and a clean surface and the input heat flux (Mayer et al., 2013):

$$R_f = \frac{T_{\partial\Omega_{h-f}} - T_{\partial\Omega_{h-f}}^0}{q} \quad (9)$$

where the temperature of the substrate-deposit interface is location dependent. Thus Eq. (9) gives a distributed fouling resistance along the heat transfer surface. An average fouling resistance can be easily quantified from surface average temperatures:

$$\bar{R}_f = \frac{\bar{T}_{\partial\Omega_{h-f}} - \bar{T}_{\partial\Omega_{h-f}}^0}{q} \quad (10)$$

RESULTS AND DISCUSSION

For HoPe and HePe systems, by solving the fully coupled governing equations together with boundary conditions given in the previous section, one can obtain the spatial distributions of the temperature, and velocity throughout the complete simulation domain. For HoIm and

HeIm systems, models introduced in Zhang et al. (2015) can be utilized to obtain the velocity and temperature distributions. Then the fouling layer structural effect on fluid flow and heat transfer can be quantitatively evaluated. Note that the dynamics of the fouling process taking into account the complex fouling layer structure will be investigated in our future work.

The fouling rig developed in Bohnet’s lab was adopted in our previous study to develop a numerical model for CaSO₄ fouling (Zhang et al., 2015). An air-foil shaped fouling layer, which is a homogeneous medium and is impermeable to the fluid (i.e., the scheme of HoIm), was eventually generated. In this work, the same type of fouling rig (but with reduced size) was investigated and the air-foil shaped fouling layer was directly adopted. The 2D geometry of the simulation system is given in Fig. 1(a) and Fig. 2. It should be noted that the porosity of the fouling layer changes with location and time. The fouling layer is not homogenous and its structure evolves as the fouling process proceeds. According to the measurement data reported in Brahim *et al.* (2004), we adopted 0.15 as the mean porosity value, which is also the value used in Zhang *et al.* (2015). The heterogeneous porous structure of the fouling layer was set to a four-layer structure based on the SEM image in Fig. 1(e). The first layer has the highest porosity value, i.e., $\omega_f=0.25$, and the fourth layer that is closest to the heat transfer surface has the lowest porosity value, i.e., $\omega_f=0.05$. The other two layers respectively have porosities of 0.2 and 0.1. As a result, the four estimated porosity values offer a volume average porosity of 0.15, which is also the porosity value for HoIm and HoPe systems. For all four systems shown in Fig. 1, the fluid inlet velocity v_{in} and the solution temperature are respectively $v_{in} = 0.1$ m/s and $T_{in} = 42$ °C. The input heat flux q is 46 kW/m². The thermal conductivities of fluid and deposit solid are respectively, 0.67 W/(m·K) and 1.3 W/(m·K). The heat capacities of fluid and solid are respectively, 4200 J/(kg·K) and 733 J/(kg·K).

Comparison of fluid flow behaviours. Our model can generate comprehensive spatial distribution data for the fluid velocity. Results for four representative systems are compared in Fig. 3.

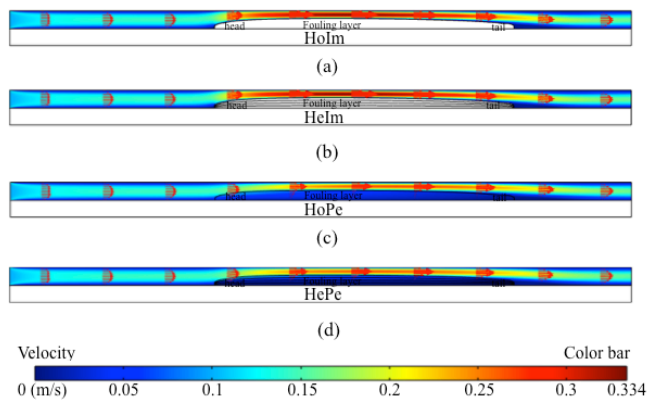


Fig. 3. Comparison of velocity distributions for different systems: (a) HoIm, (b) HeIm, (c) HoPe, and (d) HePe.

For the schemes of HoIm and HeIm, since the fouling layers are impermeable to the fluid flow, the porosity distribution in the fouling layer cannot affect the fluid flow in domain Ω_e . Fig. 3(a) and (b) thus show exactly the same velocity distribution. This observation can be confirmed by plotting the velocity profile along a cross-section-cutting line at $x=0.03$ m (see the green arrowed line in Fig. 2). Fig. 4 shows that HoIm and HeIm cases have the exactly same velocity profile. The fluid velocities in the impermeable fouling layers are zero.

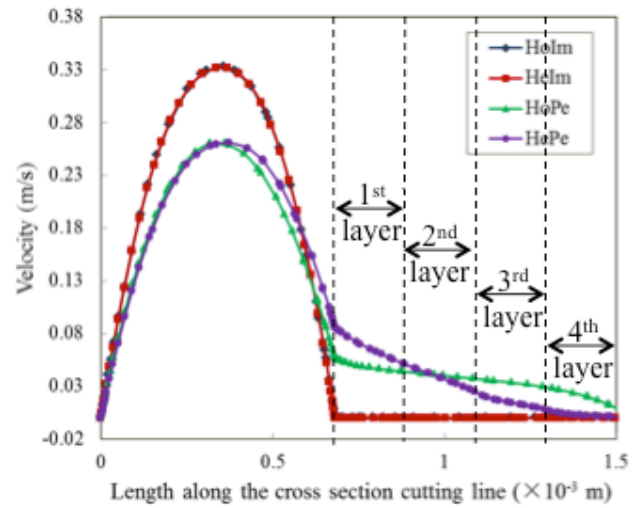


Fig. 4. The velocity distributions along the cross-section-cutting line at $x=0.03$ m for four different systems.

Simulations of permeable porous layers, however, led to drastically different flow behaviors. Velocity fields can be identified in domain Ω_f (see Fig. 3 (c) and (d)). Taking a close look at velocity profiles along the cutting line, one can observe that smooth transitions from free media flow to porous media flow were achieved for both cases of HoPe and HePe (Fig. 4). This observation implies the validity of our coupled free-porous media flow model. In the porous fouling layer, a layered structure did lead to a different velocity distribution as compared with the case with a homogeneous structure (see the comparison of HoPe and HePe in Fig. 4). Higher velocity can be identified for the 3rd and 4th layers of the deposit, in the case with a homogenous structure (see HoPe in Fig. 4). However, for a layered structure in HePe, the velocity is almost zero in the 4th layers, and it increases continuously in the 3rd, 2nd and 1st layers as the distance is further away from the substrate surface.

Comparison of heat transfer behaviours. The differences in the velocity field identified for four systems will inevitably cause different heat transfer behaviors. Temperature distributions are given in Fig. 5. Lower substrate temperatures can be readily identified for the systems with HoPe and HePe schemes (see Fig. 5 (c) and (d) and compare them with Fig. 5 (a) and (b)). The convective heat transfer arising from the porous media flow did promote heat transfer from the substrate to the fluid. The substrate in the HoPe system has the lowest temperature, since it is the only system with an appreciable

flow velocity in the fourth layer of the deposit adjacent to the substrate surface (see the curves in Fig. 4).

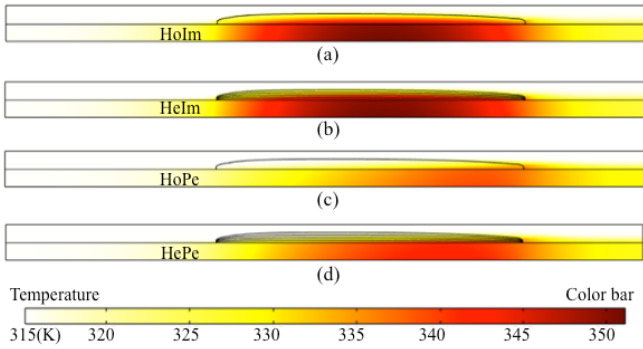


Fig. 5. Comparison of temperature distributions for different systems: (a) HoIm, (b) HeIm, (c) HoPe, and (d) HePe.

The temperature distributions along the cross-section-cutting line for four systems are given in Fig. 6. Although four systems have almost identical temperatures along the cutting line in the domain of free media flow (at some distance away from the fouling layer surface), the temperatures in the fouling layers are quite different. Two impermeable fouling layers have similar temperatures along the cutting line. The temperatures of permeable fouling layers are indeed much lower than those of impermeable fouling layers. The big temperature difference between HoPe and HePe systems results from differences in the fluid velocity field. Although two systems have the same mean porosity value, the HoPe system offers higher fluid velocity in the 3rd and 4th layers, which are locations closer to the substrate surface (see Fig. 4). Compared with the HePe system, more significant convective heat transfer at locations closer to the substrate surface leads to lower temperature in the homogenous fouling layer.

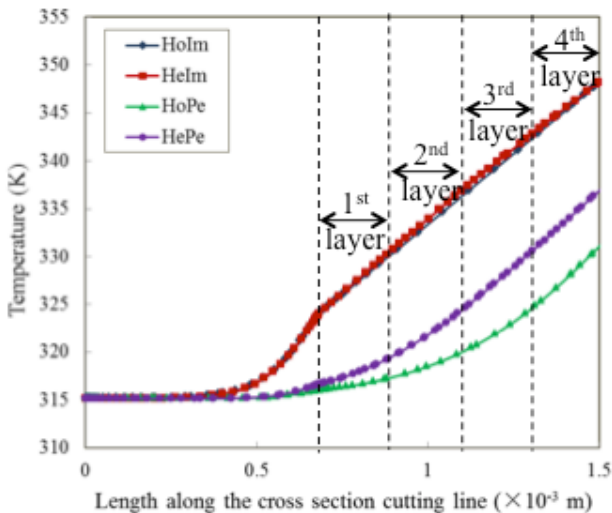


Fig. 6. The temperature distributions along the cross-section-cutting line at $x=0.03$ m for four different systems.

Since the temperature of the substrate-deposit interface directly determines the fouling resistance (see Eq. (9)), the

interface temperatures in four systems have been plotted in Fig. 7 for a comparison. For impermeable fouling layer systems, taking the layered structure into account led to negligible difference in interface temperature. Much lower interface temperatures can be identified when the deposit layers were modeled as permeable fouling layers. The temperature of a clean substrate surface without a deposit layer is also given in the same figure. It is interesting to observe that when the substrate surface is covered by a homogeneous permeable fouling layer (i.e., the HoPe system), it has localized temperatures (at locations close to the head of the air-foil shaped fouling layer) that are even lower than the clean surface temperature, indicating a negative fouling resistance.

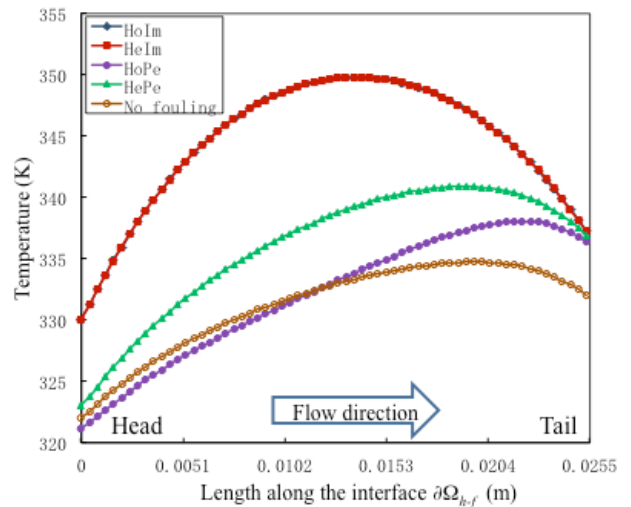


Fig. 7. Temperature profiles on the substrate-deposit interfaces for different systems.

Fouling resistance quantification. The localized fouling resistance values quantified for four systems using Eq. (9) are given in Fig. 8.

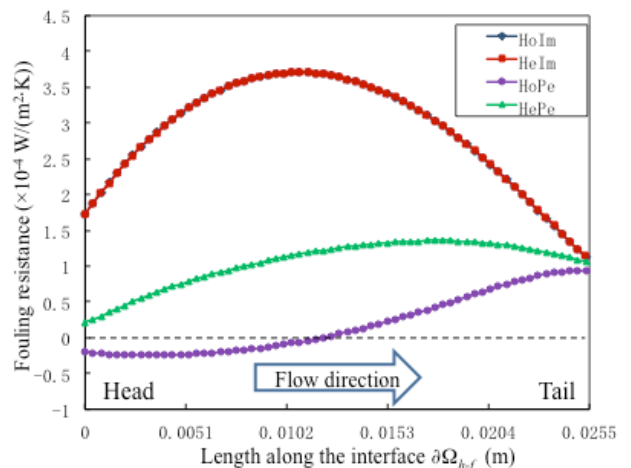


Fig. 8. Fouling resistance profiles along the substrate-deposit interface for four different systems.

Again, permeable fouling layers led to significantly lower fouling resistance values. For the system of HoPe, localized fouling resistance could even reach negative

values (see the HoPe system in Fig. 8). This part of fouling layer could promote heat transfer rather than inhibiting. Taking the layered structure into account (see the HePe system in Fig. 8), the fouling resistance became larger. However, the HoIm and HeIm systems have almost identical fouling resistance.

Figure 9 gives the average fouling resistance calculated using surface average temperatures (see Eq. (10)). The trends stated above can be identified in this Figure as well. This figure also clearly demonstrates that modeling the fouling layer using different schemes could lead to quite different fouling resistance values.

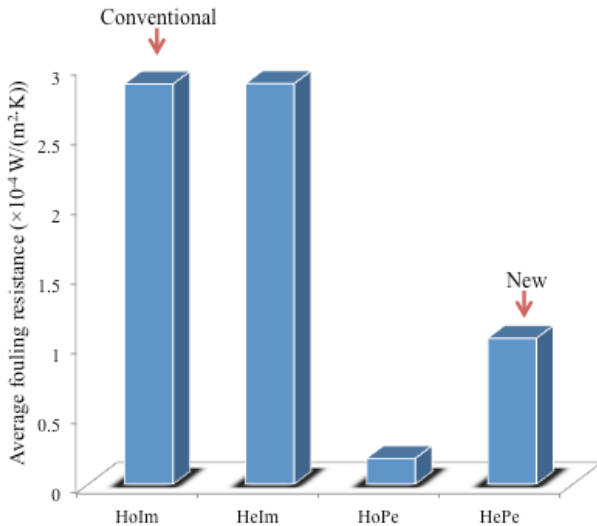


Fig. 9. Comparison of average fouling resistance values for four different systems.

Further remarks. In the introduction part, two assumptions conventionally adopted in numerical modelling of a crystallization fouling process have been stated: (1) the fouling layer is a homogeneous porous medium and (2) the layer is impermeable to the fluid flow. These two assumptions lead to the scheme of HoIm for fouling layer characterization. A relaxation of the first assumption could be realized through the incorporation of a layered structure into the fouling model (i.e., scheme HeIm). This relaxation does not affect the fluid flow behavior above the fouling layer, and has negligible effect on the substrate-deposit interface temperature and the fouling resistance. A relaxation of the 2nd assumption could be achieved by coupling free-media and porous-media flow (i.e., scheme HoPe and HePe). Drastic differences in flow and heat transfer behaviors have been observed between systems respectively with impermeable and permeable fouling layers. Convective heat transfer arising from the porous media flow can reduce the substrate-deposit interface temperature, and hence the fouling resistance.

Since the scheme of HePe can best resemble realistic fouling layer structures shown in SEM images, conventional numerical models using the HoIm scheme could have significantly overestimated the temperature of the fouling layer and hence the fouling resistance (see Fig. 9). The differences in temperature and fluid velocity distributions

between these two systems will inevitably lead to a difference in fouling kinetics, which is not investigated in this work though. It is because the temperature determines the rate constant of the surface crystallization reaction as well as the saturation concentration. The flow velocity affects the concentration distribution of dissolved salts as well as the crystal removal rate. Moreover, a major change in the deposit-solution interface may affect fouling dynamics greatly. For the scheme of HePe, the surface of pores inside the fouling layer should also be taken into account as one part of the deposit-solution interface.

It is also interesting to explore how different schemes of fouling layer characterization can affect process conditions, e.g., the pressure drop that is a critical condition for heat exchanger operations. Figure 10 shows the pressure drop between two ends of the fouling layer (see the illustration in Fig. 2). Pressure drops for systems with HoPe and HePe schemes are slightly lower than those for HoIm and HeIm systems. It is understandable that the pores in the fouling layer provide an additional path for the flow, leading to lower hydraulic resistance and hence lower pressure drop.

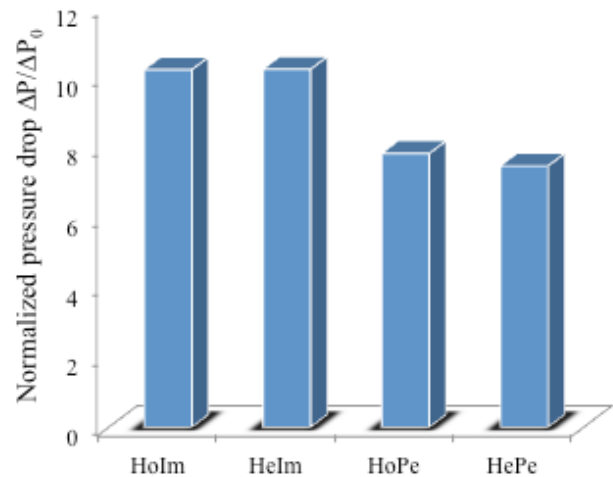


Fig. 10. Comparison of normalized pressure drop between two ends of the fouling layer for four different systems.

Moreover, it should be pointed out that the idea of treating a fouling layer as a heterogeneous porous layer permeable to the fluid as well as the modeling approach introduced in this work should be general and applicable to different sized heat exchangers.

CONCLUSIONS

The fouling layers formed on heat exchanger surfaces usually exhibit complicated structures, which evolve over time during the fouling process. How these structures can interactively affect hydrodynamics, heat and mass transfer in a heat exchanger still remains unclear. This work focuses on the identification of a reliable structural approximation scheme that can be easily incorporated into a numerical model for the growth/removal stage of the fouling process. New models that can effectively couple free media flow and porous media flow and can describe convective heat transfer

in the porous media have been developed. The new models allowed us to systematically investigate four representative structural characterization schemes, i.e., Holm, HeIm, HoPe and HePe. Simulation results demonstrated that convective heat transfer arising from porous media flow did lead to decreased temperature of the fouling layer and could reduce significantly the fouling resistance. Since the HePe scheme is the most appropriate one among four that can best capture the critical structural features of a realistic fouling layer, it should be a promising structural approximation scheme to be integrated into the next generation of numerical models for crystallization fouling.

Although the effects of fouling layer structure on momentum and heat transfer in a heat exchanger have been quantified in this work, the mass transfer and fouling kinetics haven't been explored yet. A model of dilute species transport in porous media is under development and will be integrated into the current model. Moreover, a new fouling layer growth model will be developed in the future, where the growth of a fouling layer will be characterized by the change of localized porosities. Most importantly, the current model has to be validated using experimental data, such as those on fouling resistance and pressure drop.

NOMENCLATURE

C_f	friction coefficient
C_p	specific heat capacity, J/(kg·K)
$C_{p,s}$	specific heat capacity of solid, J/(kg·K)
$C_{p,w}$	specific heat capacity of fluid, J/(kg·K)
k	permeability of the porous medium, m^2
k_0	permeability at a reference state, m^2
p	pressure, Pa
q	input heat flux, kW/m^2
R_f	fouling resistance, $m^2 \cdot K/W$
T	temperature, K
T_{in}	temperature of the inlet solution, K
$T_{\partial\Omega_{h-f}}$	temperature of substrate-deposit interface, K
$T_{\partial\Omega_{h-f}}^0$	temperature of a clean heat exchanger surface before fouling takes place, K
\vec{u}	velocity, m/s
v_{in}	inlet velocity, m/s
λ_{eq}	equivalent thermal conductivity of the fouling layer, $W/(m \cdot K)$
λ_s	thermal conductivity of the solid, $W/(m \cdot K)$
λ_w	thermal conductivity of the fluid, $W/(m \cdot K)$
μ	viscosity of the fluid, Pa·s
ρ_s	density of the deposit solid, kg/m^3
ρ_w	density of the fluid, kg/m^3
ω	porosity of the fouling layer
ω_0	porosity at a reference state
Ω_e	solution domain
Ω_f	fouling layer domain
Ω_h	metal substrate domain
$\partial\Omega_{h-f}$	substrate-fouling layer interface
$\partial\Omega_{h-e}$	substrate-solution interface

ACKNOWLEDGEMENTS

This work was supported by the Faculty Start-up Funds from Soochow University, and the research funds from the “Jiangsu Specially-Appointed Professors Program”, “Jiangsu Innovation and Entrepreneurship (ShuangChuang) Program”, National Natural Science Foundation of China (No. 21406148), Natural Science Foundation of Jiangsu Province (No. BK20130293), and the “Priority Academic Program Development (PAPD) of Jiangsu Higher Education Institutions”.

REFERENCES

- Amiri, A., Vafai, K., 1998, Transient analysis of incompressible flow through a packed bed, *Int. J. Heat and Mass Transfer*, Vol. 41, pp. 4259-4279.
- Andritsos, N., Karabelas, A.J., Koutsoukos, P.G., 1997, Morphology and structure of CaCO₃ scale layers formed under isothermal flow conditions, *Langmuir*, Vol. 13, pp. 2873-2879.
- Anwar, J., Zahn, D., 2011, Uncovering molecular processes in crystal nucleation and growth by using molecular simulation, *Angew. Chem. Int. Ed.*, Vol. 50, pp. 1996-2013.
- Bohnet, M., 1987, Fouling of heat transfer surfaces, *Chem. Eng. Technol.*, Vol. 10, pp. 113-125.
- Bohnet, M.W., 2005, Crystallization fouling on heat transfer surfaces—25 years research in Braunschweig. In: *Proceedings of 6th International Conference on Heat Exchanger Fouling and Cleaning—Challenges and Opportunities*, pp. 295–302(RP2, Article 43).
- Borisova, E.A., Adler, P.M., 2005, Deposition in porous media and clogging on the field scale, *Physical Review*, Vol. 71, pp. 016311-1-19.
- Brahim, F., Augustin, W., Bohnet, M., 2003, Numerical simulation of the fouling process, *International Journal of Thermal Sciences*, Vol. 42, pp. 323-334.
- Brahim, F., Augustin, W., Bohnet, M., 2004, Numerical simulation of the fouling on structured heat transfer surfaces, In: *Proceedings of Heat Exchanger Fouling and Cleaning: Fundamentals and Applications*, pp. 1–9 (Article 17).
- Coletti, F., Ishiyama, E.M., Paterson, W.R., Wilson, D.I., Macchietto, S., 2010, Impact of deposit aging and surface roughness on thermal fouling: distributed model, *AIChE J.*, Vol. 56, pp. 3257-3273.
- Durllofsky, L., Brady, J.F., 1987, Analysis of the brinkman equation as a model for flow in porous media, *Phys. Fluids*, Vol. 30, pp. 3329-3341.
- Ishiyama, E.M., Coletti, F., Macchietto, S., Paterson, W.R., Wilson, D.I., 2010, Impact of deposit ageing on thermal fouling: lumped parameter model, *AIChE J.*, Vol. 56, pp. 531-545.
- Ishiyama, E.M., Paterson, W.R., Wilson, D.I., 2011, Exploration of alternative models for the aging of fouling deposits, *AIChE J.*, Vol. 57, pp. 3199-3209.
- Kim, W.T., Bai, C., Cho, Y.I., 2002, A study of CaCO₃ fouling with a microscopic imaging technique, *International Journal of Heat and Mass Transfer*, Vol. 45, pp. 597-607.
- Mayer, M., Augustin, W., Scholl, S., 2013, An approach to modeling induction period in crystallization fouling, *Heat Mass Transfer*, Vol. 49, pp. 1419-1432.

Paakkonen, T.M., Riihimäki, M., Simonson, C. J., Muurinen, E., Keiski, R.L., 2012, Crystallization fouling of CaCO₃—Analysis of experimental thermal resistance and its uncertainty, *International Journal of Heat and Mass Transfer*, Vol. 55, pp. 6927-6937.

Quddus, A., Al-Hadhrami, L.M., 2009, Hydrodynamically deposited CaCO₃ and CaSO₄ scales, *Desalination*, Vol. 246, pp. 526-533.

Schoenitz, M., Grundemann, L., Augustin, W., Scholl, S., 2015, Fouling in microstructured devices: a review, *Chem. Comm.*, Vol. 51, pp. 8213-8228.

Xiao, J., Chaudhuri, S., 2012, Design of anti-icing coatings using supercooled droplets as nano-to-microscale probes, *Langmuir*, Vol. 28, pp. 4434-4446.

Yang, M., Young, A., Niyetkaliyev, A., Crittenden, B.D., 2012, Modeling fouling induction periods, *International Journal of Thermal Sciences*, Vol. 51, pp. 175-183.

Zhang, F., Xiao, J., Chen, X.D., 2015, Towards predictive modeling of crystallization fouling: A pseudo-dynamic approach, *Food and Bioproducts Processing*, Vol. 93, pp. 188-196.

Zhang, G.M., Li, G.Q., Li, W., Zhang, Z.Y., Leng, X.L., Tian, M.C., 2013, Particulate fouling and composite fouling assessment in corrugated plate heat exchangers, *International Journal of Heat and Mass Transfer*, Vol. 60, pp. 263-273.

Zhao, X., Chen, X.D., 2013, A critical review of basic crystallography to salt crystallization fouling in heat exchangers, *Heat Transfer Engineering*, Vol. 34, pp. 719-732.

Zhou, A.D., Zhang, Z.B., 2010, Fouling of calcium carbonate on the surface of sieve trays, *Ind. Eng. Chem. Res.*, Vol. 49, pp. 870-875.